

# Band topology and quantum spin Hall effect in bilayer graphene

E. Prada<sup>1</sup>, P. San-Jose<sup>2</sup> and L. Brey<sup>1</sup>

<sup>1</sup>*Instituto de Ciencia de Materiales de Madrid, (CSIC), Cantoblanco, 28049 Madrid, Spain*

<sup>2</sup>*Instituto de Estructura de la Materia (CSIC), Serrano 123, 28006 Madrid, Spain*

H.A. Fertig

*Department of Physics, Indiana University, Bloomington IN 47405*

(Dated: October 24, 2018)

We consider bilayer graphene in the presence of spin orbit coupling, to assess its behavior as a topological insulator. The first Chern number  $n$  for the energy bands of single and bilayer graphene is computed and compared. It is shown that for a given valley and spin,  $n$  in a bilayer is doubled with respect to the monolayer. This implies that bilayer graphene will have twice as many edge states as single layer graphene, which we confirm with numerical calculations and analytically in the case of an armchair terminated surface. Bilayer graphene is a weak topological insulator, whose surface spectrum is susceptible to gap opening under spin-mixing perturbations. We also assess the stability of the associated topological bulk state of bilayer graphene under various perturbations. Finally, we consider an intermediate situation in which only one of the two layers has spin orbit coupling, and find that although individual valleys have non-trivial Chern numbers, the spectrum as a whole is not gapped, so that the system is not a topological insulator.

## INTRODUCTION

The study and characterization of the properties of topological insulators has sparked considerable interest [1, 2]. A topological insulator has a bulk energy gap separating the occupied electronic bands from the empty ones. However, the conduction and valence bands in the bulk are inverted with respect to their energy position in the vacuum. This necessarily results in the existence of localized surface states that cross the energy gap and are protected by time reversal symmetry. The electronic and magnetic properties of the surface states of a three-dimensional topological insulator are chiral, and are governed by a two dimensional Dirac Hamiltonian.

In a two dimensional topological insulator the chiral surface states become helical one dimensional edge states, and at a given edge, states with opposite spin orientations transport charge in opposite spatial directions[3]. In the absence of time reversal symmetry breaking, the helicity of the edge states prevents backscattering between states in the same edge and the Hall conductivity per spin becomes quantized, although with different sign for opposite spins. Note that this system does not violate time reversal symmetry because, when reversing the time direction, both the spin and the Hall conductivity per spin reverse. In this way the total Hall conductivity of the system vanishes. As pointed out by Thouless *et al.* [4], the quantization of the Hall conductivity is a consequence of the topology of the band structure. Thouless *et al.* showed that the Hall conductivity should be an integer in units of  $e^2/h$ , i.e., a topological invariant called the first Chern number. Because the Hall conductivity per spin is quantized, two-dimensional topological insulators are also called quantum spin Hall systems. The quantum spin Hall effect was theoretically predicted [5]

to occur, and later experimentally observed [6], in HgTe quantum wells confined by CdTe barriers.

Graphene, a two-dimensional carbon crystal [7], has also been proposed to be a two-dimensional quantum spin Hall system [8–10] when the intrinsic spin orbit interaction is taken into account. Spin orbit coupling (SOC) in graphene opens a gap at the Dirac points and the system becomes a topological insulator. However, due to the  $\pi$  character of the graphene bands close to the Fermi energy, the opened gap is proportional to the square of the intra-atomic spin orbit coupling constant divided by the energy difference between the  $s$  and  $p$  orbitals of graphene [11–13]. Since carbon is a very light atom, the spin orbit gap is very small,  $\sim 10^{-3}$ meV. Consequently, the particular transport properties of graphene as a topological insulator may only be observed in extremely clean samples and at extremely low temperatures. Graphene, nevertheless, is a pedagogical toy model for analyzing properties of two-dimensional topological insulators [1].

In a Bernal stacked graphene bilayer, the conduction and the valence bands touch at two inequivalent points of the Brillouin zone and the system is a semimetal [14]. SOC in bilayer graphene also opens a gap in the band structure [15].

The spin-orbit interaction in bilayer graphene is larger, by about one order of magnitude, than in a single layer of graphene, due to the mixing of  $\pi$  and  $\sigma$  bands by the interlayer hopping [16, 17]. Nevertheless, the spin-orbit induced gap in the bilayer is small and difficult to detect experimentally. As mentioned above, our main interest in this work is the use of graphene based structures to understand properties of topological insulators. In particular, we use bilayer graphene as a model to analyze the coupling between two topological insulators.

Our aim in this work is to study the topological prop-

erties of a graphene bilayer in the presence of SOC. In graphene and bilayer graphene, the low energy properties can be described by  $2 \times 2$  Hamiltonians and for each momentum  $\vec{p}$ , the wavefunctions have a spinor form. In undoped systems, the ground state of the system can be characterized by an unit vector field,  $\vec{h}(\vec{p})$ , that indicates, at each point of the reciprocal space, the expectation value of the orientation of the pseudospin. In the reciprocal space  $\vec{h}$  has the form of a topological object. We find that in the case of graphene  $\vec{h}$  has the form of a meron, and in the case of bilayer graphene it takes the form of a double vortex meron. Thus, we find that the first Chern number of bilayer graphene is twice that of the monolayer one, and consequently the number of edge states is also doubled. In bilayers, edge states are not Kramer-protected against backscattering, which give the topological insulating phase a weak character. We also analyze the stability of the insulating bulk topology in bilayer graphene with respect to bias voltage, staggered sublattice potential and trigonal warping effects. Finally, we study a bilayer graphene system in which only a single layer has SOC. We find that this system has a finite Chern number, but is a zero gap semiconductor for which no surface states are possible.

## GRAPHENE

Carbon atoms in graphene are covalently bonded and arranged in a honeycomb lattice, which is composed of two triangular sublattices  $A$  and  $B$ . The low energy properties in graphene are mainly determined by the  $\pi$  orbitals. A tight-binding Hamiltonian with hopping  $\gamma_0$  between nearest-neighbors appropriately describes its band structure. In graphene the intrinsic SOC does not break the inversion symmetry of the honeycomb lattice and the electronic bands are spin degenerate. In addition, since the intrinsic SOC in graphene is a second order effect, the  $z$ -component of the electron spin commutes with the Hamiltonian, and the bands can be indexed by  $s_z = \pm 1$ , the up/down electron spin component perpendicular to the graphene layer. The corresponding tight binding Hamiltonian of graphene is

$$H = -\gamma_0 \sum_{\langle i,j \rangle, s_z} a_{i,s_z}^\dagger b_{j,s_z} + it_{so} \sum_{\langle\langle i,j \rangle\rangle, s_z} s_z \nu_{ij} c_{i,s_z}^\dagger c_{j,s_z}. \quad (1)$$

Here  $a_{i,s_z}$  ( $b_{i,s_z}$ ) annihilates an electron on sublattice  $A$  ( $B$ ) at site  $i$  and spin  $s_z$ ,  $t_{so}$  is the next-nearest neighbor spin orbit hopping amplitude and  $c_j$  is either  $a_j$  or  $b_j$ , depending whether the index  $j$  labels an  $A$  or  $B$ -sublattice site, respectively. The factor  $\nu_{ij}$  is  $+1$  if the next-nearest neighbor hopping path rotates counterclockwise and  $-1$  if it rotates clockwise.

In undoped graphene, and for  $t_{so} = 0$ , the conduction and valence bands touch at two inequivalent points of

the Brillouin zone:  $\mathbf{K} = \frac{4}{3}\frac{\pi}{a}(1,0)$  and  $\mathbf{K}' = -\frac{4}{3}\frac{\pi}{a}(1,0)$ , being  $a$  the lattice parameter of the triangular lattice. These are known as Dirac points. The main effect of the SOC in the electronic spectrum is the opening of a energy gap,  $6\sqrt{3}t_{so}$ , at the Dirac points. Near these points the wave functions for each spin  $s_z$  can be expressed via the  $\mathbf{k} \cdot \mathbf{P}$  approximation [18] in terms of envelope functions  $\psi_{+,s_z} = [A_{s_z}(\mathbf{r}), B_{s_z}(\mathbf{r})]$  and  $\psi_{-,s_z} = [A'_{s_z}(\mathbf{r}), B'_{s_z}(\mathbf{r})]$  for states near the  $\mathbf{K}$  and  $\mathbf{K}'$  points respectively. These wavefunctions satisfy the Dirac equations  $H_{\tau_z, s_z} \psi_{\tau_z, s_z} = \varepsilon \psi_{\tau_z, s_z}$ , where  $\tau_z = \pm 1$  specifies the Dirac points  $\mathbf{K}$  and  $\mathbf{K}'$  and

$$H_{\tau_z, s_z} = v_F(p_x \tau_z \sigma_x + p_y \sigma_y) + \Delta_{so} \sigma_z \tau_z s_z. \quad (2)$$

Here  $v_F = \frac{\sqrt{3}}{2} \gamma_0 a$ ,  $\Delta_{so} = 3\sqrt{3}t_{so}$  and  $\sigma_i$  are Pauli matrices representing the pseudospin degree of freedom corresponding to the two sites per unit cell of the graphene lattice. Note that  $\vec{p}$  denotes the distance in momentum from the  $\mathbf{K}$  and  $\mathbf{K}'$  points. It is important to note that for a given  $s_z$ , the Dirac mass terms in the Hamiltonian induced by SOC at  $\mathbf{K}$  and  $\mathbf{K}'$  have the same magnitude but different sign.

Graphene with intrinsic SOC is a topological insulator with a finite spin Hall conductivity. For a given  $s_z$  and valley index  $\tau_z$ , the spin Hall conductivity as obtained from the Kubo formula has the form

$$\sigma_{xy}^{s_z, \tau_z} = 2 \frac{e^2}{\Omega} \sum_{\vec{k}, i, j} \frac{\text{Im}[\langle \psi_k^i | v_y | \psi_k^j \rangle \langle \psi_k^j | v_x | \psi_k^i \rangle]}{(\varepsilon_k^i - \varepsilon_k^j)^2}, \quad (3)$$

where  $j(i)$  runs over occupied (empty) states,  $v_\nu$  is the velocity operator in the  $\nu$  direction and the wavefunctions  $\psi_k^i$  and energies  $\varepsilon_k^i$  are obtained by diagonalizing Eq. (2) for the corresponding  $\tau_z$  and  $s_z$ . In undoped graphene (Fermi energy crossing the Dirac points), the Hall conductivity *for each valley* takes the value

$$\sigma_{xy}^{s_z, \tau_z} = -\frac{1}{2} \frac{e^2}{h} s_z, \quad (4)$$

where  $h$  is the Planck constant. When summing over spins the total Hall conductivity of the system is zero, as it should be for a system with time reversal symmetry [1, 2]. However, for each spin the Hall conductivity is quantized, although with opposite sign. This is the signature of the quantum spin Hall effect. Note also that although for an isolated valley the Hall conductivity is a half integer in units of  $e^2/h$ , the sum of the  $\mathbf{K}$  and  $\mathbf{K}'$  conductivities is quantized to integer multiples of  $e^2/h$ , as it should be for a filled band of noninteracting electrons [4, 19]. In an insulator, the value of the Hall conductivity in units of  $e^2/h$  is related to the first Chern number [4] of its bandstructure. The Chern number corresponding to a  $2 \times 2$  Hamiltonian

$$H_{\tau_z, s_z} = \varepsilon(\vec{p}) \vec{h}(\vec{p}) \cdot \vec{\sigma}, \quad (5)$$

is related to the number of times the unit sphere is covered by the unit vector  $\vec{h}(\vec{p})$  when  $\vec{p}$  runs over the whole reciprocal space [1, 2, 20]. This number takes the form

$$n = \frac{1}{4\pi} \int d^2p (\partial_{p_x} \vec{h} \times \partial_{p_y} \vec{h}) \cdot \vec{h}, \quad (6)$$

where  $\vec{h}(\vec{p})$  depends on  $\tau_z$  and  $s_z$  and  $\pm\epsilon(\vec{p})$  are the energy eigenvalues.  $n$  is a topological invariant, the Pontryagin index of the mapping  $h(\vec{p})$  [20]. Physically, the vector  $\vec{h}(\vec{p})$  represents the expectation value of the orientation of the pseudospin associated with the wavefunctions of the Hamiltonian, Eq. (2).

The vector  $\vec{h}$  defines the topology of the band structure and may be written in the form

$$\vec{h} = \left[ \tau_z \sqrt{1 - [h_z(p)]^2} \cos \theta, \sqrt{1 - [h_z(p)]^2} \sin \theta, h_z(p) \right], \quad (7)$$

with  $h_z(p) = s_z \tau_z \Delta_{so} / \sqrt{v_F^2 p^2 + \Delta_{so}^2}$ . Here the valley index  $\tau_z = \pm$  defines the right and left vorticity of the topological structure and  $\theta$  is the azimuthal angle made by the momentum vector  $\vec{p}$ . At asymptotically large momentum,  $h_z$  vanishes, while in the cortex core we have  $h_z = \tau_z s_z$ . This implies that there are four flavors of topological objects which are usually referred to as merons [21, 22], since they are essentially half skyrmions. The four possible merons are illustrated in Fig. 1. The Chern number index corresponding to the field  $\vec{h}$  takes the form

$$n = \frac{\tau_z}{4\pi} \int_0^\infty d^2p \frac{1}{p} \frac{dh_z}{dp} = -\tau_z \frac{1}{2} h_z(0) = -\frac{1}{2} s_z. \quad (8)$$

Thus, the topological charge corresponding to each Dirac point is  $\pm 1/2$  depending on the sign of the electron spin. When summing over the contribution from both Dirac points the Chern number in graphene is  $\pm 1$ . This result follows from the fact that, topologically, a meron has half the winding number of a skyrmion, that is, the topological object formed by the two Dirac points together.

### Helical Edge States

The most spectacular consequence of the existence of an insulator with a topologically non trivial band structure is the appearance of gapless conducting states at interfaces where the topology of the band structure changes. In two dimensional quantum spin Hall systems, helical edge states appear at the surfaces of the material. At each edge there exists a pair of one dimensional channels with opposite spins that propagate in opposite directions. In graphene these states have been obtained numerically by diagonalizing nanoribbons terminated with different geometries, zigzag[10, 23] or armchair[24]. Here we describe analytically how helical

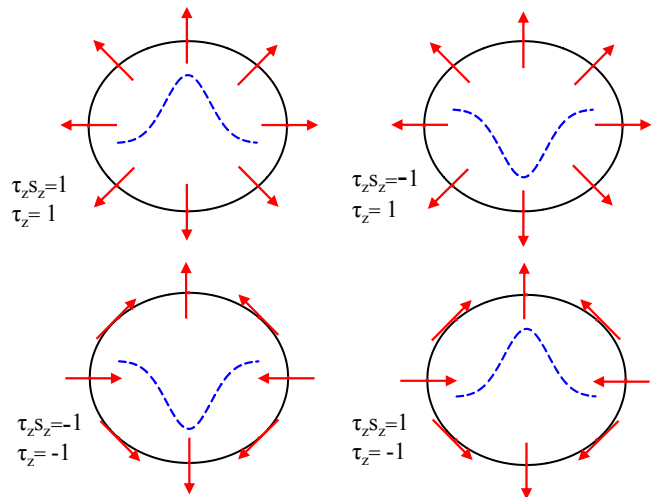


FIG. 1: (Color online) Four flavors of merons, see Ref. 21. These are vortices that are right or left handed depending on the valley index  $\tau_z$ . The topological charge,  $\pm 1/2$ , is determined by the sign of the spin  $s_z$ .

one dimensional channels appear at an armchair terminated edge.

We consider an edge running along the  $\hat{y}$ -direction and the vacuum region is defined by the  $x < 0$  condition. The graphene armchair termination consists of a line of  $A$ - $B$  dimers, so it is natural to have the wave function amplitude vanish on both sublattices at  $x = 0$ . To do this we must admix valleys[25] and require

$$\begin{aligned} A_{s_z}(x=0) + A'_{s_z}(x=0) &= 0 \quad \text{and} \\ B_{s_z}(x=0) + B'_{s_z}(x=0) &= 0. \end{aligned} \quad (9)$$

Note that the boundary conditions should be satisfied by each spin separately. We consider solutions with momentum  $p_y$  along the surface and energy  $E$  inside the gap,  $|E| < \Delta_{so}$ , where  $p_x = i\hbar\kappa$ . The general solution has the form

$$\left[ \alpha \begin{pmatrix} \sin \xi \\ \cos \xi \end{pmatrix} e^{iK_x x} + \beta \begin{pmatrix} \sin \xi' \\ \cos \xi' \end{pmatrix} e^{iK'_x x} \right] e^{i\frac{p_y}{\hbar} y} e^{-\kappa x} \quad (10)$$

with  $\hbar v_F \kappa = \sqrt{\Delta_{so}^2 - E^2 + v_F^2 p_y^2}$  and

$$\tan \xi = i \frac{v_F (\hbar\kappa - p_y)}{E - \Delta_{so} s_z} \quad \text{and} \quad \tan \xi' = -i \frac{v_F (\hbar\kappa + p_y)}{E + \Delta_{so} s_z}. \quad (11)$$

The boundary conditions, Eq. (9), imply that  $\tan \xi = \tan \xi'$ . This, together with the definition of  $\kappa$ , gives the solutions

$$E = s_z v_F p_y \quad \text{and} \quad \hbar v_F \kappa = \Delta_{so}. \quad (12)$$

Since the graphene flake exists in the  $x > 0$  region, normalizability of the wavefunction implies that  $\kappa$  should be

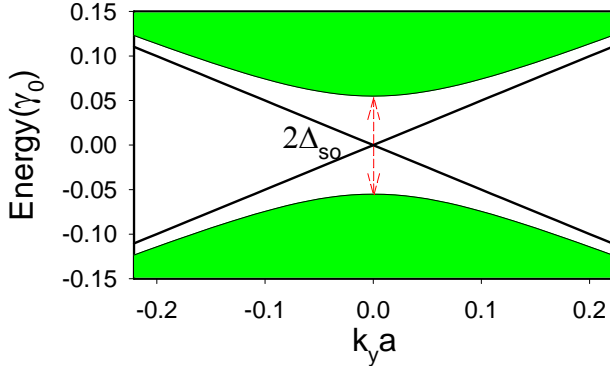


FIG. 2: (Color online) Tight-binding band structure of an armchair terminated wide nanoribbon. Shadow regions represent bulk states.

positive for any spin. Therefore, quasiparticles with positive spin,  $s_z > 0$ , move in the positive  $\hat{y}$  direction and have an energy  $E = v_F p_y$ . On the contrary, quasiparticles with  $s_z < 0$  move in the negative  $\hat{y}$  direction and have energy  $E = -v_F p_y$ . On the opposite surface, for which the wavefunction exists for  $x < 0$ , normalizability implies that  $p_x = -i\hbar\kappa$ . In this case  $E = -s_z v_F p_y$ , and the edge states with positive (negative) velocity in the  $\hat{y}$ -direction have  $s_z < 0$  ( $s_z > 0$ ). In Fig. 2 we plot the band structure of a wide armchair terminated nanoribbon with a SOC  $t_{so} = 0.01\gamma_0$ .

## GRAPHENE BILAYERS

Bilayer graphene consists of two stacked graphene sheets. In bilayer graphene there are four sites per unit cell, which we label  $A_1$ ,  $B_1$  and  $A_2$  and  $B_2$  in the first and second layer respectively. We consider the so-called Bernal stacking, commonly found experimentally, in which site  $B_2$  is exactly on top of the sublattice  $A_1$ . Interlayer coupling is modeled by hopping amplitude  $\gamma_1$  between these two sites in each unit cell. The low energy properties of this model are well described for each spin  $s_z$  by the following Hamiltonian acting on the four-component spinor  $(A_1, B_1, A_2, B_2)$  [14],

$$H_{\tau_z, s_z}^{BG} = \mathcal{T}_0 \otimes H_{\tau_z, s_z} - \frac{\gamma_1}{2} (\mathcal{T}_x \otimes \sigma_x - \mathcal{T}_y \otimes \sigma_y) \quad , \quad (13)$$

where  $H_{\tau_z, s_z}$  is the monolayer Hamiltonian of Eq. (2),  $\sigma_i$  and  $\mathcal{T}_i$  are the Pauli matrices for the sublattice and layer degree of freedom respectively and  $\mathcal{T}_0$  is the unit matrix in the layer subspace. The four energy bands of  $H^{BG}$ ,

denoted by  $\varepsilon_{\pm}^{(1,2)}(p)$ , are

$$\varepsilon_{\pm}^{(\alpha)} = \pm \sqrt{v_F^2 p^2 + \Delta_{so}^2 + \frac{\gamma_1^2}{2} + (-1)^\alpha \sqrt{v_F^2 p^2 \gamma_1^2 + \frac{\gamma_1^4}{4}}} \quad (14)$$

These energies are independent of  $s_z$  and  $\tau_z$  [26]. The eigenvalues  $\varepsilon_{\pm}^{(2)}$  describe two strong interlayer coupling bands with energies  $\varepsilon_+^{(2)} \geq \gamma_1$  and  $\varepsilon_-^{(2)} \leq -\gamma_1$ . These bands do not touch at the Dirac points, and correspond to wavefunctions mostly localized at sites  $A_1$  and  $B_2$ , which form strong dimers [27]. The eigenvalues  $\varepsilon_{\pm}^{(1)}$  describe low energy bands. Performing the usual low energy approximation  $v_F p \ll \gamma_1$ , the dispersion of these bands can be approximated by  $\varepsilon_{\pm}^{(1)} = \pm \sqrt{\frac{p^4}{4m^2} + \Delta_{so}^2}$ , where  $m$  is an effective mass induced by the interlayer hopping,  $m = \gamma_1/2v_F^2$ . The corresponding low energy eigenstates are mostly localized at sites  $B_1$  and  $A_2$ . All of these states are degenerate in the spin  $s_z$  and valley  $\tau_z$  indices.

For a given  $s_z$  and  $\tau_z$ , the Hall conductivity can be obtained numerically by plugging the eigenvalues and eigenfunctions of the Hamiltonian (13) into the expression (3). For charge-neutral bilayer graphene, only negative energy bands are filled, and the Hall conductivity takes the form

$$\sigma_{xy}^{s_z, \tau_z} = -\frac{e^2}{h} s_z \quad (15)$$

When summing over the valleys, the Hall conductivity per spin is twice that of graphene. Interestingly, this is the same result one would expect for the case of two decoupled layers, although the eigenfunctions are completely different from those of the coupled bilayer. As in the case of a monolayer, time reversal symmetry dictates opposite  $\sigma_{xy}^{s_z, \tau_z}$  upon reversing the spin, so that the total Hall conductivity of the system is zero.

## Band structure topology

The value of the Hall conductivity can be understood from the topology of the band structure through the first Chern number. Because of the gap  $\sim 2\gamma_1$  between the high energy dimer bands  $\varepsilon_{\pm}^{(2)}$ , these cannot change their topology by adding a weak SOC. Therefore, only the gapless  $\varepsilon_{\pm}^{(1)}$  bands acquire non-trivial topology that contributes to a finite Chern number  $n$ . To compute  $n$ , it is then sufficient to consider the effective  $2 \times 2$  low energy Hamiltonian that describes the low energy bands of the system in the limit  $\varepsilon \ll \gamma_1$  [14],

$$\begin{aligned} H_{\tau_z, s_z} &= \begin{pmatrix} \Delta_{so} \tau_z s_z & -\frac{(\tau_z p_x - i p_y)^2}{2m} \\ -\frac{(\tau_z p_x + i p_y)^2}{2m} & -\Delta_{so} \tau_z s_z \end{pmatrix} \\ &= \Delta_{so} \tau_z s_z \sigma_z - \frac{(p_x^2 - p_y^2)}{2m} \sigma_x - \frac{p_x p_y}{m} \tau_z \sigma_y \quad . \quad (16) \end{aligned}$$

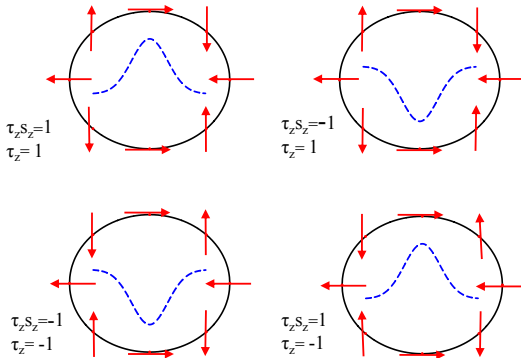


FIG. 3: (Color online) Four flavors of double vortex merons. These are vortices that are right or left handed depending on the valley index  $\tau_z$ . The topological charge  $\pm 1$  is determined by the sign of the spin.

This Hamiltonian acts on the two-component spinor  $(B_1, A_2)$ . This Hamiltonian describes the low energy effective coupling between carbon atoms in different layers which are not directly connected by tunneling. Their coupling arises as a result of virtual transitions through the high energy dimer states that have been integrated out. From this Hamiltonian and the relation of Eq. (5) we get the following expression for the unit vector field  $\vec{h}(\vec{p})$ :

$$\vec{h} = \left[ -\sqrt{1 - [h_z]^2} \cos 2\theta, -\tau_z \sqrt{1 - [h_z]^2} \sin 2\theta, h_z \right], \quad (17)$$

with  $h_z(\vec{p}) = \Delta_{so} \tau_z s_z / \sqrt{\Delta_{so}^2 + \left(\frac{p^2}{2m}\right)^2}$ . As in the case of a monolayer, the valley index  $\tau_z$  determines the vorticity of the field  $\vec{h}(\vec{p})$  and the angle  $\theta$  is the azimuthal angle of momentum  $\vec{p}$ . At large momentum  $p$ , the  $\hat{z}$ -component of the field  $\vec{h}$  vanishes and the field is confined to be in the  $x - y$  plane. As in the case of the monolayer, there are four flavors of these topological objects, shown in Fig. 3. The Chern number of the corresponding fields  $\vec{h}(\vec{p})$  is

$$n = 2 \frac{\tau_z}{4\pi} \int_0^\infty d^2 p \frac{1}{p} \frac{dh_z}{dp} = -\tau_z h_z(0) = -s_z. \quad (18)$$

Thus, the Chern number corresponding to each valley is  $\pm 1$  depending on the sign of the electron spin. It is interesting to note that, although these objects have twice the Pontryagin charge of merons (which are often thought as half a skyrmions), they are not skyrmions. Far away from the center of a skyrmion, i.e., at  $p \rightarrow \infty$ , the orientation of the vector field  $\vec{h}(\vec{p})$  is constant. This is not the case of bilayer graphene (see Fig. 3), although, as in a skyrmion, the Chern number is unity for each  $\tau_z, s_z$ . We call these objects double vortex merons. When summing

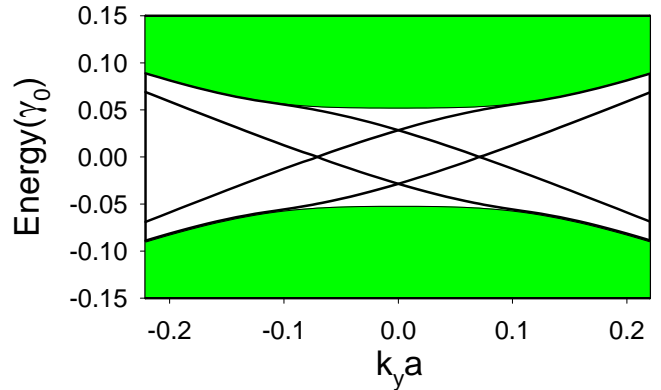


FIG. 4: (Color online) Band structure of a wide armchair terminated bilayer graphene ribbon for a single spin. The (green) shaded areas represent the continuum bulk states.

over valleys the Chern number in bilayer graphene is  $\pm 2$  (depending on the spin), in agreement with the results obtained for the Hall conductivity.

### Edge states

According to the bulk-boundary correspondence rule [1], and since the Chern number of bilayer graphene is twice that of the monolayer, the number of helical surface states should also be double. In order to analyze the edge states, we diagonalize the tight-binding Hamiltonian corresponding to a wide armchair terminated bilayer graphene ribbon. In Fig. 4 we plot its band structure as function of the wavevector  $k_y$  along the ribbon for a given electron spin  $s_z$ . As in the case of a monolayer of graphene, the Hamiltonian commutes with  $s_z$  and the band structure is degenerate in spin. The bulk bands are indicated by shaded regions. We identify two pairs of parallel edge states inside the gap. The states with positive velocity are located on the opposite ribbon edge from the states with negative velocity. This can be seen by analyzing the eigenfunctions of the low-energy Hamiltonian, Eq. (16). As a result of the helicity of the edge states, their location changes to the opposite edge when the spin of the carriers changes sign.

Bilayer graphene edge states can be understood as bonding/antibonding combinations of the surface states of the two constituent graphene layers. In the absence of tunneling between the graphene layers, the surface states have the form of Eq. (10) with  $\xi, \xi', E$  and  $\kappa$  determined by Eq. (11) and Eq. (12). For finite  $\gamma_1$ , surface states from layers 1 and 2 become coupled. To leading order in  $\gamma_1$ , the energies and wavefunctions of the graphene

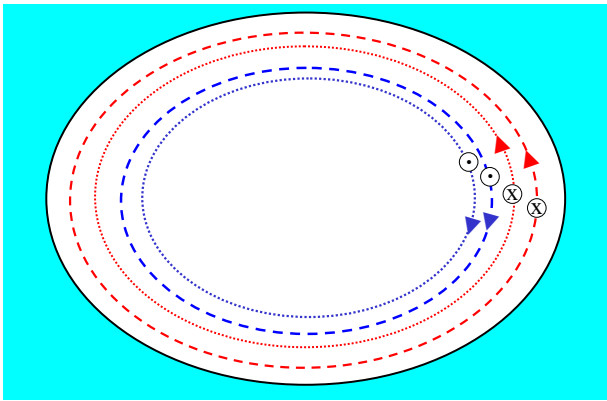


FIG. 5: (Color online) Schematic diagram of the edge states in a bilayer graphene system. At the edge of the sample there are four channels: two with spin up and moving in one direction, and two with spin down and moving in the opposite direction. Dotted and dashed lines represent channels formed by bonding/antibonding combinations of individual layers edge channels.

bilayer Hamiltonian Eq. (13), defined for  $x < 0$ , are

$$E_{\pm}^{s_z} = s_z v_F p_y \mp \frac{\gamma_1}{4} \quad (19)$$

$$\psi_{\pm}^{s_z} = \frac{1}{2\sqrt{2}} \begin{pmatrix} -i s_z \\ 1 \\ \pm s_z \\ \pm i \end{pmatrix} \left[ e^{iK_x x} - e^{iK'_x x} \right] e^{ik_y y} e^{-\Delta_{so} x / \hbar v_F} \quad (20)$$

where  $\pm$  correspond to bonding/antibonding states. These expressions are valid when the SOC  $\Delta_{so}$  is much larger than  $\gamma_1/4$ . In other situations, bulk states should reduce the bonding/antibonding energy separation.

By inspection of Eq. (20), we see that at each edge of the system there exist four one dimensional channels: two with spin up moving in one direction and the other two with spin down and moving in the opposite direction, see Fig. 5. The two terminal electrical conductance in this model is  $4e^2/h$ . The injection of charge current through edge states would result in antisymmetric spin accumulation at the edges. In a four terminal geometry the spin conductances should be quantized.

However, in bilayer graphene, backscattering between channels at the same edge moving in opposite directions with opposite spins is not forbidden, in contrast to the case of monolayer graphene. Indeed, Kramer's theorem ensures degeneracy of time-reversed pairs in the absence of time reversal symmetry breaking, preventing backscattering between energy degenerate edge states with opposite spins at high symmetry points of the Brillouin zone, such as the  $\Gamma$ -point (for which  $\vec{k} = -\vec{k}$  modulo a reciprocal lattice vector) [1]. While in monolayer graphene edge states branches cross at the  $\Gamma$ -point  $k_y = 0$ , bilayer graphene edge state branches cross away from  $k_y = 0$ , see

Fig. 4. As a result, SOC perturbations will in general split their degeneracy, and open a gap in the edge state dispersion around zero energy. Therefore, this model is not, strictly speaking, a topological insulator, since there exist single-body effects that are symmetric under time reversal that can induce backscattering between edge channels, and make the edges insulating. This happens for any two-dimensional insulator with an even number  $N_K$  of edge state pairs, related by time reversal symmetry ( $k_y, s_z \rightarrow -k_y, -s_z$ ), at any given energy inside the gap ( $N_K = 2$  for the case at hand). An odd number of pairs  $N_K$ , like in monolayers or trilayers with SOC, implies that there exists at least one of those pairs crossing at a high symmetry point, and are therefore protected from scattering by Kramer's theorem. A  $\mathbb{Z}_2$  topological invariant of the form

$$\nu = N_K \bmod 2, \quad (21)$$

is defined [1] to differentiate strict topological insulators (dubbed 'strong'),  $\nu = 1$ , from 'weak' topological insulators, with  $\nu = 0$  and  $N_K \neq 0$ . Within this classification, bilayer graphene is a weak topological insulator. The 'weakness' is in relation to the class of time-reversal-invariant perturbations that can open a gap in the edge states, in this case general spin-mixing perturbations.

### Stability of the topological insulating phase

The non-trivial insulating phase created by the intrinsic SOC may be destroyed by Rashba SOC or other perturbations if they are strong enough. This happens not by inducing backscattering between edge states, but by band reconnection, which changes the topology of the bulk bandstructure back to that of a conventional insulator [9]. It is a generic possibility both in weak and strong topological insulators.

We now consider the destruction of bilayer graphene's topological insulator phase by a symmetric Rashba SOC, a staggered sublattice mass term and a voltage bias between the two layers. We also discuss the effect of the trigonal warping on the topological insulating phase.

1) The *Rashba spin orbit coupling* term arises due to an electric field perpendicular to the bilayer plane or from the interaction with a substrate,

$$H_R = \lambda_R \mathcal{T}_0 \otimes (\tau_z \sigma_x \otimes s_y - \sigma_y \otimes s_x). \quad (22)$$

Here  $s_x$  and  $s_y$  are the Pauli matrices in the spin subspace and  $\lambda_R$  is the intensity of the coupling. This term violates mirror symmetry about the planes. In the presence of this term the  $z$ -component of the electron spin is not conserved, but there is a region of values of the coupling,  $0 < \lambda_R < \Delta_{so}$ , for which the ground state is adiabatically connected[9, 10] to the topological insulating phase. For values of the coupling  $\lambda_R > \Delta_{so}$  the



energy gap closes and the electronic structure is that of a zero gap semiconductor with quadratically dispersive bands.

2) A *staggered sublattice potential* of the form

$$H_v = \lambda_v \mathcal{T}_0 \otimes \sigma_z \quad (23)$$

stabilizes the band insulator phase that competes with the topological insulating phase. This term is typically zero in graphene but would be present for a similar boron nitride film. In the effective  $2 \times 2$  Hamiltonian this term appears as a mass term independent of the spin and valley,  $\lambda_v \sigma_z$ . In the presence of this term, the form of the unit vector field  $\vec{h}(\vec{p})$  of Eq. (17) is unaffected, but now the  $z$ -component takes the form

$$h_z(p) = \frac{\Delta_{so} \tau_z s_z + \lambda_v}{\sqrt{(\Delta_{so} \tau_z s_z + \lambda_v)^2 + \left(\frac{p^2}{2m}\right)^2}}. \quad (24)$$

The Chern number associated with this vector field  $\vec{h}(\vec{p})$  is

$$n = -\tau_z \text{sign}(\Delta_{so} \tau_z s_z + \lambda_v) \quad (25)$$

For values  $\lambda_v < \Delta_{so}$  the Chern number is  $-s_z$  (equal for both valleys) and the system is a topological insulator. For values  $\lambda_v > \Delta_{so}$  we have  $n = -\tau_z$  and the total Chern number per spin is zero when summing over valleys. In this case the bilayer graphene becomes a band insulator.

3) A *bias voltage* between the layers gives a contribution to the bilayer Hamiltonian, Eq. (13), of the form

$$H_{bias} = V \mathcal{T}_z \otimes \sigma_0. \quad (26)$$

This term acts equally on both sublattices and on both spin orientations. In the effective  $2 \times 2$  low energy Hamiltonian Eq. (16), this term has exactly the same form as the staggered sublattice potential  $V \sigma_z$ . Thus, the condition for the existence of a topological insulating phase in the bilayer is  $V < \Delta_{so}$ .

In the last two cases, when  $\lambda_v > \Delta_{so}$  or  $V > \Delta_{so}$ , the system becomes a conventional insulator with vanishing Hall and spin Hall conductances. The two inequivalent valleys, considered independently, have nonzero topological charge with opposite sign,  $n = -\tau_z$ , and a valley dependent Hall effect may occur [28]. The nonzero Chern number of each valley induces chiral modes in topological domain walls in graphene [29] and bilayer graphene [30].

4) *Trigonal warping*. The inclusion in the Hamiltonian of bilayer graphene of a weak direct  $A_2$ - $B_1$  hopping term  $\gamma_3 \ll \gamma_1$  introduces in the  $2 \times 2$  effective Hamiltonian a term of the form

$$H_w = v_3 (\tau_z p_x \sigma_x - p_y \sigma_y), \quad (27)$$

with  $v_3 = \frac{\sqrt{3}}{2} a \gamma_3 / \hbar$ . This term produces a trigonal warping in the band structure, which stretches the isoenergy

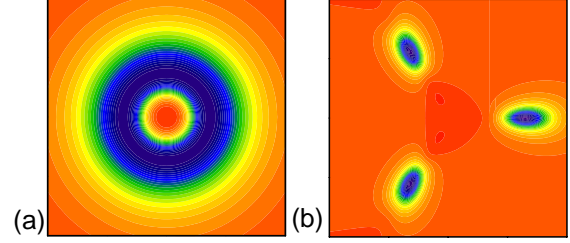


FIG. 6: (Color online) Density plot in the reciprocal space of the integrand of Eq. (18) in the absence (a) and the presence (b) of trigonal warping. The center of each square corresponds to the original Dirac point at  $\mathbf{K}$ . Cold colors represent regions where the integrand is bigger. The parameters used in these plots are  $\gamma_1 = 0.1\gamma_0$ ,  $\Delta_{so} = 10^{-5}\gamma_0$  and in (b)  $\gamma_3 = 0.05\gamma_0$ .

lines along the directions  $\phi = 0, \frac{2}{3}\pi$  and  $\frac{4}{3}\pi$  for the valley  $\mathbf{K}$  and along the directions  $\phi = \frac{1}{3}\pi, \pi$  and  $\frac{5}{3}\pi$  for the valley  $\mathbf{K}'$  [27]. For  $\Delta_{so} = 0$ , the trigonal warping produces a dramatic change in the band structure. For a given valley, instead of two parabolic bands touching at the Dirac point, there are now four Dirac points, one at the center ( $\mathbf{K}$  or  $\mathbf{K}'$ -point), and three others that occurs at finite momentum and in the directions  $\phi$  mentioned above. The SOC opens gaps at the four Dirac points, making the system insulating. To analyze the nature of the insulating phase we compute the Chern number. The warping term breaks the symmetric form of the unit vector field  $\vec{h}(\vec{p})$  given in Eq. (17) and prevents an analytical calculation of the Chern number. By integrating numerically Eq. (3) we obtain that the Chern number is not affected by the trigonal warping. In the absence of trigonal warping the main contribution to the integral comes from an annulus around each Dirac point where  $dh_z/dp$  is maximum, see Fig. 6(a) (dark region). When the trigonal warping effects are taken into account, the main contribution to the Chern number comes from the regions around the three new Dirac points, Fig. 6(b).

## SPIN-ORBIT PROXIMITY EFFECT

In this Section we analyze the case of a graphene bilayer in which only one of the layers has a finite intrinsic SOC  $\Lambda_{so}$ , whereas the other layer has zero coupling. This could happen in a bilayer in contact with a strong SOC metal [31], or in a bilayer where heavy atoms or molecules have been deposited on top of one of the two layers [32].

When only one of the layers is affected by the SOC, the  $2 \times 2$  effective Hamiltonian takes the form

$$H_{\tau_z, s_z} = \begin{pmatrix} \Delta_{so} \tau_z s_z & -\frac{(\tau_z p_x - i p_y)^2}{2m} \\ -\frac{(\tau_z p_x + i p_y)^2}{2m} & 0 \end{pmatrix}$$

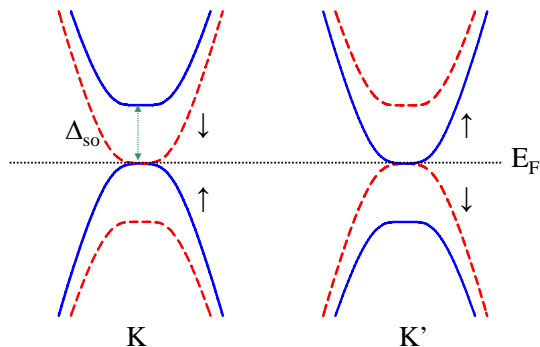


FIG. 7: (Color online) Low energy band structure of a graphene bilayer where only one of the two layers has an finite SOC  $\Delta_{so}$ . Left and right panels correspond to the bands near the  $\mathbf{K}$  and  $\mathbf{K}'$  points, respectively. Bands for states with spin up  $s_z = 1$  (down  $s_z = -1$ ) are represented with solid (dashed) lines. The Fermi energy is indicated by an dotted horizontal line. The SOC opens a gap  $\Delta_{so}$  with a different sign for each valley and each spin orientation.

$$= \frac{\Delta_{so}}{2} \tau_z s_z (\sigma_0 + \sigma_z) - \frac{(p_x^2 - p_y^2)}{2m} \sigma_x - \frac{\tau_z p_x p_y}{m} \sigma_y \quad (28)$$

and the unit vector field  $\vec{h}$  has almost the same form as in Eq. (17). Thus, the Chern number of this system is equal to that of a graphene bilayer with intrinsic SOC in both layers,

$$n = -s_z. \quad (29)$$

Although from the value of the Chern number the system appears to be a topological insulator, this is not the case: it turns out it is not a true insulator at all. From the diagonalization of the Hamiltonian of Eq. (28) we get the band dispersion

$$\varepsilon_{\pm} = \frac{\Delta_{so} \tau_z s_z \pm \sqrt{\Delta_{so}^2 + \frac{p^4}{4m^2}}}{2}. \quad (30)$$

This band structure, shown in Fig. 7, corresponds to an indirect zero band gap semiconductor. The absence of SOC in one of the layers breaks the inversion symmetry, making the bands non-degenerate under independent inversion of valley and spin. When both valleys and/or both spins are considered, there is no gap in the spectrum. However, for each spin and valley there is an energy gap  $\Delta_{so}$  at  $\vec{p} = 0$ , and the system is thus an insulator from an *optical* point of view. Moreover, if the system is free from perturbations that mix the two valleys and the two spins, it will also behave as an effective electronic insulator. This has an important consequence on the existence of surface states in the bilayer structure. In zigzag edge terminations for which it is not necessary to admix valleys to satisfy the boundary

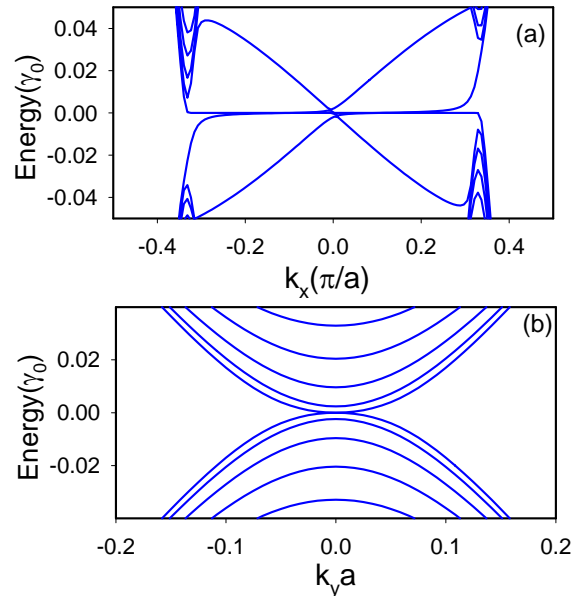


FIG. 8: (Color online) Tight binding band structure of a zigzag (a) and an armchair (b) terminated bilayer graphene nanoribbon in which there is SOC only in one of the layers. These results correspond to  $s_z=1$ . Results for  $s_z=-1$  are obtained by changing  $\vec{k}$  to  $-\vec{k}$ . In the numerics  $\gamma_1 = 0.1\gamma_0$  and  $\Delta_{so} = 3\sqrt{3} \times 10^{-2}\gamma_0$ . The width of the armchair and zigzag nanoribbons is  $151a$  and  $120\sqrt{3}a$  respectively. In the armchair case all the states are extended across the ribbon. In the zigzag one the states in the center of the Brillouin zone are localized at the edges.

conditions[25], states coming from different valleys can be treated independently and dispersive surface localized channels appear in the spectrum, see Fig. 8(a). However, for armchair terminated ribbons where, in order to satisfy the boundary conditions, the wavefunctions have to be a linear combination of both valleys, no localized surface states appear in the band structure, see Fig. 8(b). The absence of a full energy gap and the lack of surface states in some boundary terminations are clear indicators that a graphene bilayer with SOC in only one layer is not a quantum spin Hall system.

## CONCLUSION

In this work we reviewed the description of single layer graphene with SOC as a topological insulator in terms of the first Chern number, which arises naturally in the computation of the Hall conductivity. We showed then that the Chern number per spin in bilayer graphene is two, twice that of the monolayer. This doubling is reflected also in the number of topological surface states,



as a consequence of the bulk-surface correspondence rule. By numerically computing the spectrum of finite size samples, we checked that bilayer systems have twice as many edge states as a monolayer. This was furthermore confirmed analytically in the case of surfaces with arm-chair termination. The fact that the total Chern number per spin is even means that the bilayer system is a weak topological insulator, susceptible to gap opening if the system is subject to spin-mixing perturbations (such as a weak Rashba SOC). We also assessed the general stability of the bulk topological insulating state of bilayer graphene with respect to Rashba SOC, a staggered sublattice potential, interlayer bias, and trigonal warping. The first three perturbations compete with the intrinsic SOC and, when sufficiently large, spoil the inverted gap property that is crucial to making the system a topological insulator. Finally, we examined a bilayer graphene system in which only one layer has intrinsic SOC. Although in this system individual valleys have non-trivial Chern numbers, the spectrum as a whole is not gapped, so that the system is not a topological insulator.

*Note added:* While this manuscript was in the final stage of preparation, a manuscript by Cortijo, Grushin and Vozmediano appeared[33] which studies the Chern Simons coefficients in graphene and bilayer graphene using an effective action formalism.

### Acknowledgments

Funding for the work described here was provided by MICINN-Spain via grants FIS2009-08744 (EP and LB) and FIS2008-00124 (PSJ), and by the NSF through Grant No. DMR-1005035 (HAF).

---

[1] M. Z. Hasan and C. L. Kane, *Topological insulators* (2010), URL <http://www.citebase.org/abstract?id=oai:arXiv.org:1002.3895>.

[2] X.-L. Qi and S.-C. Zhang, *Physics Today* **63**, 33 (2010).

[3] For simplifying the discussion, here we consider systems for which the  $z$ -component of the spin commutes with the Hamiltonian.

[4] D. J. Thouless, M. Kohmoto, M. P. Nightingale, and M. den Nijs, *Phys. Rev. Lett.* **49**, 405 (1982).

[5] B. A. Bernevig, T. L. Hughes, and S.-C. Zhang, *Science* **314**, 1757 (2006).

[6] M. König, S. Wiedmann, C. Brune, A. Roth, H. Buhmann, L. W. Molenkamp, X.-L. Qi, and S.-C. Zhang, *Science* **318**, 766 (2007).

[7] A. H. Castro-Neto, F. Guinea, N.M.R. Peres, K.S. Novoselov, and A.K. Geim, *Rev. Mod. Phys.* **81**, 109 (2009).

[8] F. D. M. Haldane, *Phys. Rev. Lett.* **61**, 2015 (1988).

[9] C. L. Kane and E. J. Mele, *Phys. Rev. Lett.* **95**, 226801 (2005).

[10] C. L. Kane and E. J. Mele, *Phys. Rev. Lett.* **95**, 146802 (2005).

[11] D. Huertas-Hernando, F. Guinea, and A. Brataas, *Phys. Rev. B* **74**, 155426 (2006).

[12] H. Min, J. E. Hill, N. A. Sinitsyn, B. R. Sahu, L. Kleinman, and A. H. MacDonald, *Phys. Rev. B* **74**, 165310 (2006).

[13] Y. Yao, F. Ye, X.-L. Qi, S.-C. Zhang, and Z. Fang, *Phys. Rev. B* **75**, 041401 (2007).

[14] E. McCann and V. I. Fal'ko, *Phys. Rev. Lett.* **96**, 086805 (2006).

[15] R. van Gelderen and C. M. Smith, *Phys. Rev. B* **81**, 125435 (2010).

[16] F. Guinea, *Spin-orbit coupling in a graphene bilayer and in graphite* (2010), URL <http://www.citebase.org/abstract?id=oai:arXiv.org:1003.1618>.

[17] H.-W. Liu, X. C. Xie, and Q. feng Sun, *Giant intrinsic spin-orbit coupling in bilayer graphene* (2010), URL <http://www.citebase.org/abstract?id=oai:arXiv.org:1004.0881>.

[18] T. Ando, *J. Phys. Soc. Jpn.* **74**, 777 (2005).

[19] N. A. Sinitsyn, J. E. Hill, H. Min, J. Sinova, and A. H. MacDonald, *Phys. Rev. Lett.* **97**, 106804 (2006).

[20] R. Rajaraman, *Solitons and Instantons* (North-Holland, The Netherlands, 1982).

[21] S.M. Girvin and A.H. MacDonald, *Perspectives in Quantum Hall Effects* (Wiley-Interscience, 1997).

[22] L. Brey, H. A. Fertig, R. Côté, and A. H. MacDonald, *Phys. Rev. B* **54**, 16888 (1996).

[23] W. Li and R. Tao, *Edge states in monolayer and bilayer graphene* (2010), URL <http://www.citebase.org/abstract?id=oai:arXiv.org:1001.4168>.

[24] M. Zarea and N. Sandler, *Phys. Rev. Lett.* **99**, 256804 (2007).

[25] L. Brey and H. Fertig, *Phys. Rev. B* **73**, 235411 (2006).

[26] If in the bilayer system, apart from the SO term, we also include a mass term coming from a bias voltage  $V$  between layers, the eigenvalues would depend on  $s_z$  and  $\tau_z$  in the form  $[\varepsilon^{(\alpha)}]^2 = v_F^2 p^2 + \Delta_{so}^2 + \frac{V^2}{4} \frac{\tau_z^2}{2} + (-1)^\alpha \sqrt{\gamma_1^2 (v_F^2 p^2 + \tau_z s_z V \Delta_{so}) + V^2 (v_F^2 p^2 + \Delta_{so}^2) + \frac{\gamma_1^4}{4}}$ .

[27] E. McCann, D. S. Abergel, and V. I. Fal'ko, *Solid State Communications* **143**, 110 (2007).

[28] D. Xiao, W. Yao, and Q. Niu, *Phys. Rev. Lett.* **99**, 236809 (2007).

[29] W. Yao, S. A. Yang, and Q. Niu, *Phys. Rev. Lett.* **102**, 096801 (2009).

[30] I. Martin, Y. M. Blanter, and A. F. Morpurgo, *Phys. Rev. Lett.* **100**, 036804 (2008).

[31] Y. S. Dedkov, M. Fonin, U. Rüdiger, and C. Laubschat, *Phys. Rev. Lett.* **100**, 107602 (2008).

[32] A. H. Castro Neto and F. Guinea, *Phys. Rev. Lett.* **103**, 026804 (2009).

[33] A. Cortijo, A. G. Grushin, and M. A. H. Vozmediano (2010), URL <http://www.citebase.org/abstract?id=oai:arXiv.org:1007.3704>.